Design by analysis of deep-sea type III pressure vessel

Jantara Junior, Valter; Papaelias, Mayorkinos

DOI:
10.1016/j.ijhydene.2020.12.128

Document Version
Peer reviewed version

Citation for published version (Harvard):
Jantara Junior, V & Papaelias, M 2021, 'Design by analysis of deep-sea type III pressure vessel', *International Journal of Hydrogen Energy*, vol. 46, no. 17, pp. 10468-10477. https://doi.org/10.1016/j.ijhydene.2020.12.128

Design by analysis of deep-sea type III pressure vessel

Valter Luiz Jantara Junior*, Mayorkinos Papaelias

School of Metallurgy and Materials, University of Birmingham, Birmingham, UK

Abstract

This paper explores the potential of hydrogen as an energy carrier for deep-sea applications. Finite element analysis of a type III pressurised cylinder to the intended working pressures of 300 bar internal and up to 600 bar external were carried out for different designs and safety factors. Design parameters such as helical angle, liner, helical, and hoop thicknesses were studied and optimised. A buckling analysis was carried out for the optimised designs and recommendations to increase the maximum allowable external pressure are given.

Keywords:

deep-sea pressure vessel, nonlinear buckling analysis, finite element analysis, eigenvalue analysis, design by analysis

Data statement

The raw (finite element models) and processed data are open and fully available at Ref. [1].

1. Introduction

Hydrogen is an energy carrier with significant potential as an alternative to conventional fossil fuels and batteries. There are different methods for hydrogen storage including pressure vessels, cryogenic tanks and various metal hydrides

*Corresponding author

Email address: v.l.jantarajunior@bham.ac.uk (Valter Luiz Jantara Junior)

[2]. Each of the aforementioned storage methods has its own advantages and disadvantages. Thus, in choosing the most appropriate hydrogen storage approach, the intended application and its nature should be taken into consideration beforehand. The volume versus energy density requirements of the application as well as the type of use (i.e. interrupted or continuous hydrogen consumption for power generation) need to be determined [3]. So far the majority of the applications have focused on the use of pressurised gas cylinders for hydrogen storage. These can be categorised in five types based on their characteristics. Type I pressurised gas cylinders are made of aluminium or steel. Type II pressurised gas cylinders are made of steel or aluminium with glass, aramid, or carbon filament winding added around the metal (in the hoop area only). Type III pressurised gas cylinders are made of a glass fibre/aramid or carbon fibre filament wound composite wrapped around the entirety of the pressure vessel, with a steel or aluminium liner. Type IV pressurised gas cylinders are made of carbon fibre reinforced composite with a thermoplastic polymer liner [4]. More recently, Type V pressurised gas cylinders have been developed from a composite material without lining [5].

Pressurised hydrogen gas cylinders have been studied extensively in recent years, with the main application focus being primarily related to automotive [6] and secondarily, to decentralised power generation for backup power. The use of pressurised hydrogen gas cylinders in maritime transport applications has been considered previously to a limited extent. However, no studies presently exist on the design requirements and performance of pressurised hydrogen gas cylinders exposed to a deep underwater operating environment, with external pressure greater than 150 bar.

Several authors have studied methods to improve the design and lifetime of pressurised gas cylinders [7, 8, 9, 10, 11, 12, 13, 14]. Zhang et al. [15] review different failure prediction and analysis methods for composite pressurised gas cylinders, but the literature on externally loaded pressurised gas cylinders is scarce, particularly when deep-sea applications are concerned, as most of the studies focus on pressures external pressures of 120 bar or below.

Laboratory tests performed on composite cylinders under hydrostatic pressure showed that finite element analysis could predict the buckling loads accurately [16, 17]. Hernández-Moreno et al. [18] chose two different winding patters for a composite cylinder under hydrostatic pressure. They observed no influence of the winding pattern on the buckling behaviour. The use of sliding stiffeners, on the other hand, can increase the buckling resistance up to 41% when compared with a conventional unstiffened cylinder made of aluminium [19]. Cai et al. [20] employed the reliability-based load and resistance factor design (LRFD) method to design a type III pressure vessel for subsea applications subjected to an external pressure of 120 bar. Molavizadeh and Abdolmajid [21] employed finite element analysis in order to optimise the geometry and winding angle of a composite pressure vessel. They found out that a winding angle of 45° was the optimum angle for a geodesic filament winding pattern, and estimated failure based on the progressive failure criterion.

With the increasing use of hydrogen by underwater Automated Unmanned Vehicles (AUVs) and submarines as an alternative energy source to batteries, there is an increasing need to better understand the design requirements for pressurised gas cylinders subjected to greater pressure and establish accurately appropriate safety factors and margins of safety before widespread commercial use can be achieved.

The present paper provides for the first time a detailed investigation of the loading characteristics and design requirements for a Type III pressurised gas cylinder exposed to significant external loads during deep underwater operation.

2. Finite element setup

To optimise the space in the autonomous underwater vehicle (AUV), the pressure vessel was designed with a cylinder radius of 150 mm and length of 800 mm (internal dimensions), as shown in Figure 1. Hemispherical domes with the radius of 150 mm form the dome. A type III pressure vessel (aluminium liner fully wrapped by carbon fibre composite [22]) was chosen to withstand the

intended working pressure of 300 bar.

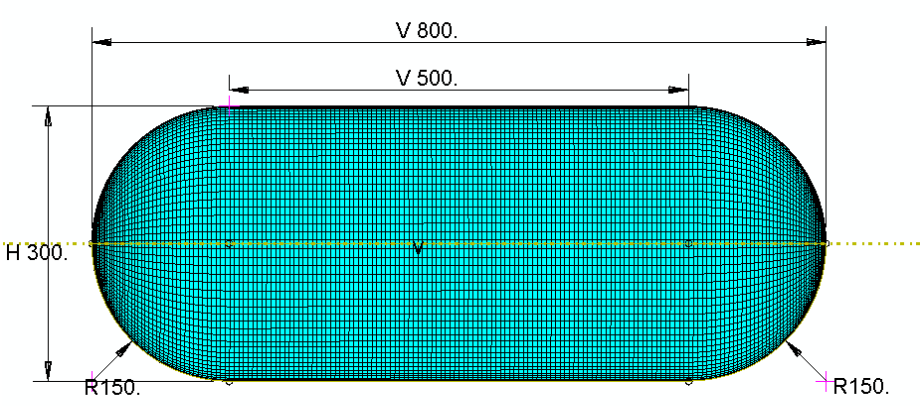

Figure 1: Drawing showing dimensions and finite element mesh of pressure vessel, units in mm.

The commercial finite element code SIMULIA Abaqus 2017 [23] was used in this research study. The liner material of choice was aluminium 7075-T6 with a Johnson-Cook plastic constitutive rule. The parameters used are shown in Table 1. The wrapping composite material employed was T700 carbon fibre/epoxy composite. Table 2 and Table 3 show the material parameters for the composite.

Table 1: Material parameters for aluminium 7075-T6 [24].

Elastic parameters		Johnson-Cook parameters		
Young's modulus (GPa)	Poisson's ratio	A (MPa)	B (MPa)	n
71.7	0.33	473	210	0.3813

Table 2: Elastic material parameters for for T700 fibre/epoxy [14].

Young's modulus (GPa)			Shear modulus (GPa)			Poisson's ratio		
E_x	E_y	E_z	G_{xy}	G_{xz}	G_{yz}	ν_{xy}	ν_{xz}	ν_{yz}
141	11.4	11.4	7.1	7.1	7.1	0.28	0.28	0.4

Table 3: Strength material parameters for for T700 fibre/epoxy [14].

Strength parameters (MPa)				
Fibre direction		Transversal direction		Shear
Tensile strength (X^T)	Compressive strength (X^C)	Tensile strength (Y^T)	Compressive strength (Y^C)	Shear strength (S)
2080	1250	60	290	110

The composite layers were added as a composite layup on top of the liner (and thus the interface between layers is assumed perfectly bonded) using the same mesh as the liner. Additional layers with different orientations were added as required, each corresponding to one composite ply. The cross-sectional behaviour between plies was calculated from section integration points during the analysis.

First, a mesh convergence analysis was performed in order to define the final mesh to be used in all subsequent simulations. The pressure vessel was designed with full integration linear shell elements (S4), and this element type was used in all subsequent simulations, including linear and non-linear analysis. The converged mesh had a total of 19,992 elements. The failure criterion chosen in this study was the maximum stress failure criterion. This choice was based on the study by Rafiee and Torabi [25] where they have compared several failure criteria to the experimental results from refs. [26, 27]. They have found that the maximum stress failure criterion was the closest to the experimental data.

The maximum stress failure criterion (f) is shown in Equation 1, where σ_x is the stress in the fibre direction, σ_y is the stress in the transversal direction, and σ_{xy} is the shear stress [28]. It is a noninteractive theory, meaning that the

interaction between different stress components is not considered.

$$f = \max\left(\frac{\sigma_x}{X^T}, \frac{\sigma_x}{X^C}, \frac{\sigma_y}{Y^T}, \frac{\sigma_y}{Y^C}, \frac{|\sigma_{xy}|}{S}\right) \tag{1}$$

In this mesh convergence study, the stacking sequence of the composite was antisymmetric ($[+\alpha,-\alpha]_{n/2}$) with the helical angle (α) being 45° and no liner material nor composite hoop (90°) layers present. The number of helical layers (n) was 80, resulting in a thickness of 40 mm as each layer is 0.5 mm thick. The vessel was subjected to the internal working pressure of 300 bar. The mesh convergence analysis (Figure 2) shows convergence is achieved to less than 0.1% with around 20,000 elements. The element size for this mesh is 5 mm. Three integration points were used per layer. The converged mesh is shown in Figure 1.

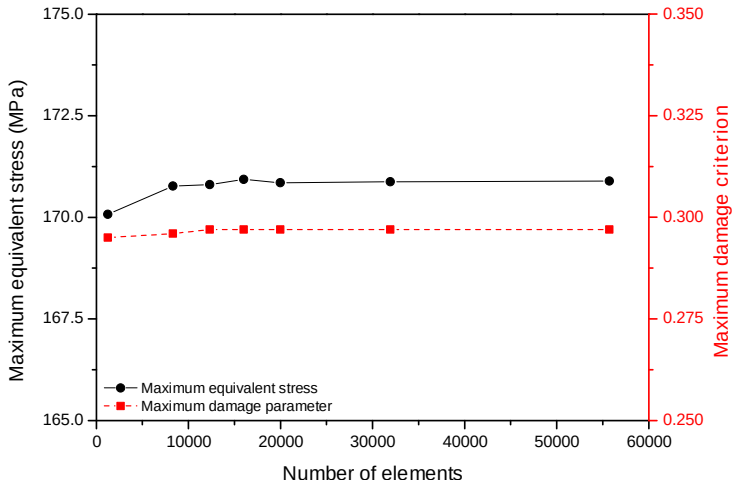

Figure 2: Maximum stress and maximum damage criterion as a function of number of elements showing convergence at around 20,000 elements.

In the next section of this study, several parameters are varied and studied, such as the helical angle, number of helical layers, number of hoop layers, and liner thickness. For simplification, 10 different designs were selected, based on the liner thickness and whether or not reinforcing composite hoop layers are present. In this sensitivity study, the winding angles were varied 5° increments

and the composite layer thickness was fixed at 0.5 mm. Whenever present, the hoop layers were always added after all the helical layers. The helical layer stacking sequence is always antisymmetric. The 10 chosen designs are shown in Table 4.

Table 4: Configuration of different designs considered.

Design #	Liner thickness (mm)	Reinforcing hoop layer
1A	0.0	✗
2A	2.5	✗
3A	5.0	✗
4A	7.5	✗
5A	10.0	✗
1B	0.0	✓
2B	2.5	✓
3B	5.0	✓
4B	7.5	✓
5B	10.0	✓

3. Results and discussion

3.1. Design optimisation

The main objective of the design optimisation is to find the thinnest configuration for each design of the pressure vessel able to withstand the working pressure of 300 bar safely, thus maximising the volume of hydrogen per cylinder and consequently the AUV autonomy. The optimisation was carried out by first reducing the number of helical layers, followed by the hoop layers, if these are present. Two different versions of each design were designed, for safety factors of 2.25 (fail pressure of 675 bar) and 3.0 (fail pressure of 900 bar). The safety factor (SF) was calculated according to Equation 2 [13]. These different versions will allow a more complete understanding of the buckling behaviour of different

designs, calculated in the next subsection.

$$\mathrm{SF} = \frac{1}{f} \tag{2}$$

In order to find the optimum design for each version, a parametric study was conducted. The results for designs 1A to 5A (without hoop reinforcement) are shown in Figure 3. As expected, Figure 3a shows that increasing the thickness of either the liner or helical layer increases the safety factor of the pressure vessel of all simulated helical angles. Figure 3b, on the other hand, shows the optimal helical angle for different designs. For a safety factor of 2.25, the helical angle of 50° is optimum for designs 1A, 2A, and 3A. The angle of 55° takes over as the optimum helical angle for pressure vessels with liners of 7.5 mm (4A) and 10 mm (5A). For a safety factor of 3.0, the helical angle of 50° is optimum in all cases, except for design 5A, where an angle of 55° is optimum.

The same analysis was carried out for designs containing hoop reinforcement (1B to 5B). The results for a safety factor of 2.25 and 3.0 are shown in Figure 4a and 4b, respectively. Note that the helical layer thickness was fixed, and the specific dimensions can be seen in Tables 5 and 6. Differently from the pressure vessels without hoop reinforcement, when hoop layers are present, the helical angle of 45° was found to always be the optimum helical angle. For the 45° case, the safety factor increases as the number of hoop layers increase, until a maximum value is reached. At this point, increasing the hoop layers will not significantly increase the safety factor. On the other hand, helical angles of 50° and 55° show an inverted parabolic relationship with hoop layer thickness. Initially, for these angles, the cylinder area of the pressure vessel is the weakest part of the pressure vessel. Hence, increasing the number of hoop layers will increase the safety factor. This is true until a certain point, which is when the dome area of the pressure vessel overcomes the cylinder as the weakest part. This happens in the transition area between the cylinder and the dome, as shown in Figure 5. For the helical angle of 45° the transition between cylinder and dome is almost imperceptible. As the helical angle increases, however, so does the failure criterion between dome and cylinder. Helical angles of 40° and

60° were also simulated for the hoop reinforced designs. However, as the safety faction was always lower than 2.0, these are not shown.

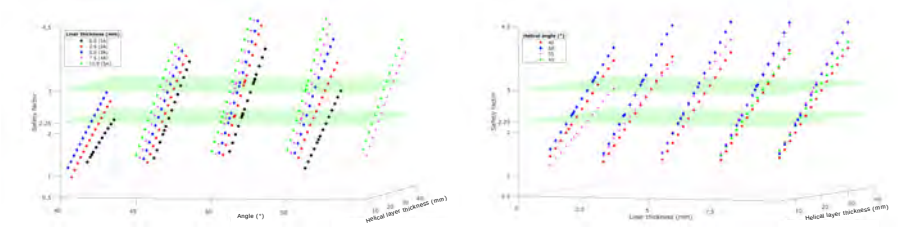

(a) (b)

Figure 3: Safety factor for designs without hoop reinforcement as a function of: (a) helical thickness and helical angle, and (b) helical thickness and liner thickness.

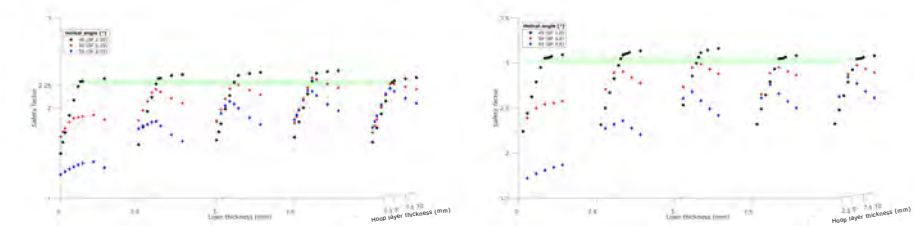

(a) (b)

Figure 4: Safety factor for designs with hoop reinforcement as a function of liner thickness and hoop layer thickness, aiming for a safety factor of 2.25 (a), and 3.0 (b). The helical thickness of each design can be seen in Tables 5 and 6. Refer to the dataset [1] for the interactive version of the graph.

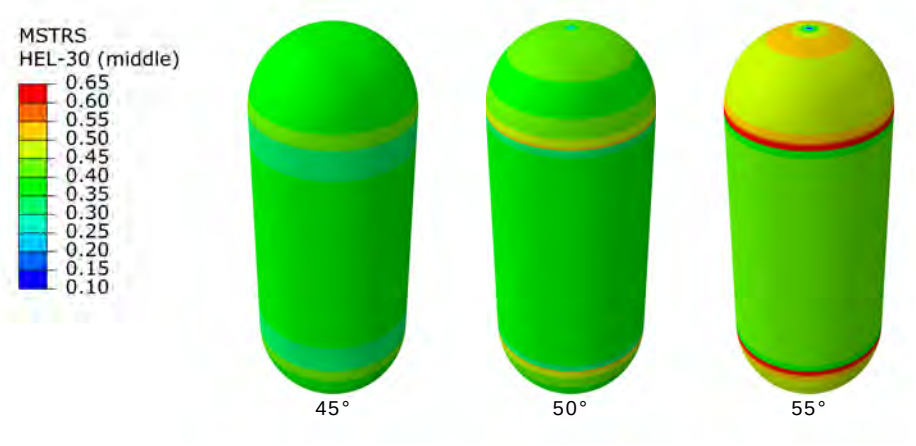

Figure 5: Maximum stress contour plot of the last helical ply (in contact with first hoop ply) for design 2B, safety factor 3.0, at different helical angles. Refer to the dataset [1] for the interactive version of the graph.

We have simulated around 800 different configurations in order to obtain the final optimised designs, for the two different safety factors. The final optimised dimensions are shown in in Tables 5 and 6. It can be seen that the total thickness will usually decrease as the liner thickness increase, whereas the weight increases. The only exception is the linerless design without hoop reinforcement (1A) which is the heaviest for both safety factors, as shown in Figure 6. In addition, the designs that contain the hoop reinforcement are lighter than their counterparts without reinforcement. This is due to the fact that the reinforcing material is only employed in the most critical area of the vessel, which is the cylinder.

Table 5: Optimised parameters for all designs (safety factor of 2.25).

Design	Liner thickness (mm)	Helical thickness (mm)	Hoop thickness (mm)	Helical angle	Dome thickness (mm)	Cylinder thickness (mm)	Weight (kg)
1A	0.0	24.5	-	50	24.5		33.6
2A	2.5	19.0	-	50	21.5		31.4
3A	5.0	16.0	-	50	21.0		32.5
4A	7.5	13.0	-	55	20.5		33.7
5A	10.0	10.0	-	55	20.0		34.9
1B	0.0	18.0	4.5	45	18.0	22.5	28.6
2B	2.5	15.0	4.5	45	17.5	22.0	29.7
3B	5.0	12.0	4.0	45	17.0	21.0	30.5
4B	7.5	8.5	5.0	45	16.0	21.0	31.8
5B	10.0	5.5	4.5	45	15.5	20.0	32.6

Table 6: Optimised parameters for all designs (safety factor of 3.0).

Design	Liner thickness (mm)	Helical thickness (mm)	Hoop thickness (mm)	Helical angle	Dome thickness	Cylinder thickness	Weight (kg)
1A	0.0	33.0	-	50	33.0		45.3
2A	2.5	26.0	-	50	28.5		41
3A	5.0	23.0	-	50	28.0		42.4
4A	7.5	20.0	-	50	27.5		43.4
5A	10.0	17.0	-	55	27.0		44.5
1B	0.0	24.0	6.0	45	24.0	30.0	38.1
2B	2.5	21.0	5.5	45	23.5	29.0	38.8
3B	5.0	18.0	5.5	45	23.0	28.5	40
4B	7.5	14.5	6.0	45	22.0	28.0	40.9
5B	10.0	11.0	6.0	45	21.0	27.0	41.4

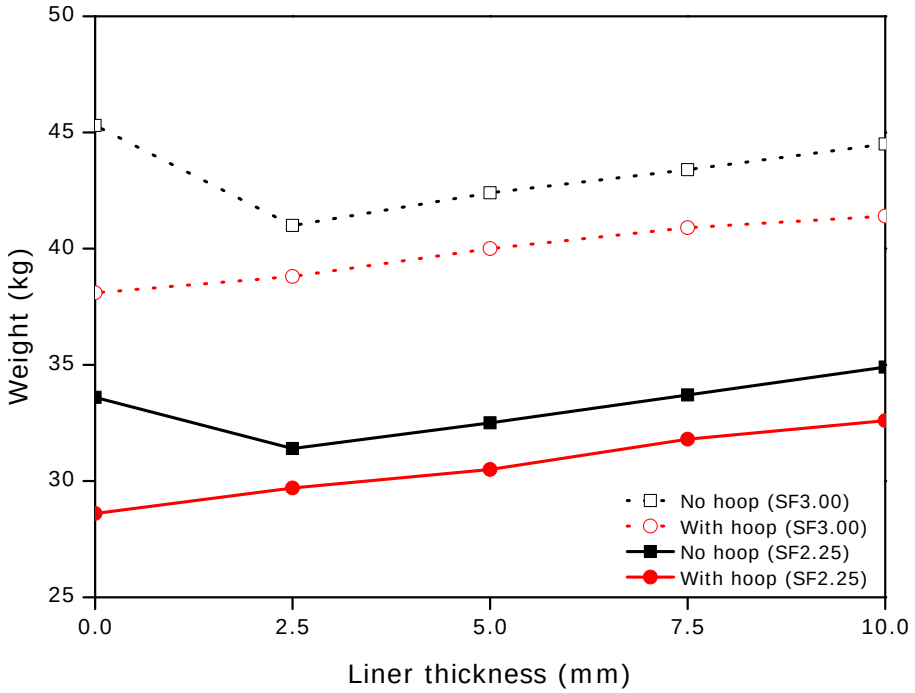

Figure 6: Weight versus liner thickness for the optimised designs in Tables 5 and 6.

The Von Mises stress contour plots can be seen in Figures 7 and 8 for designs without and with hoop reinforcement, respectively. As expected, we can see higher stresses for the version with a safety factor of 2.25 as there is less reinforcing material in these configurations. In all cases, the internal stress tends to decrease as the liner thickness increases. The cylinder is always the most stressed part of the pressure vessel.

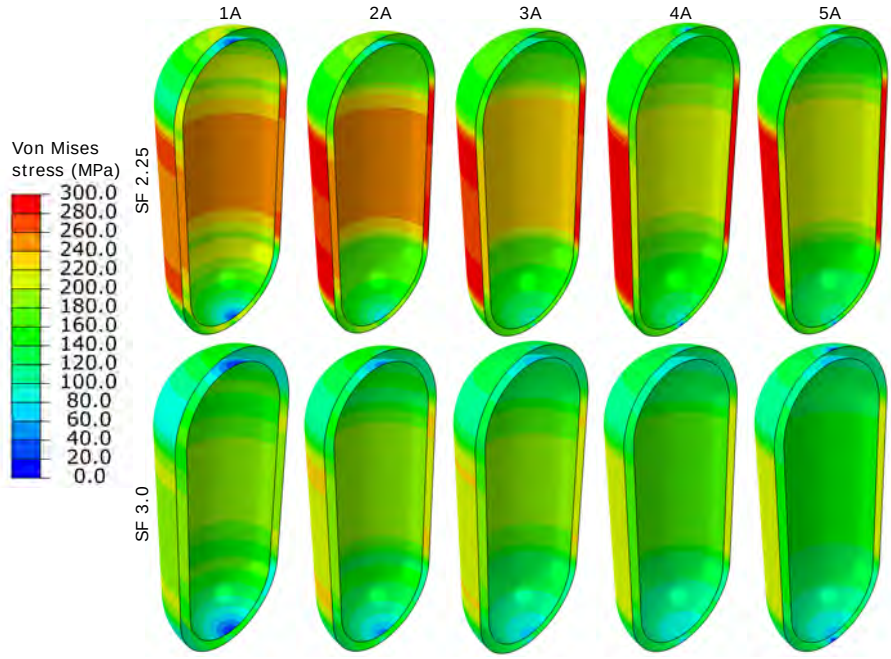

Figure 7: Von Mises stress contour plots for the first and last material layers for designs without hoop reinforcements for both safety factors subjected to 300 bar internal pressure.

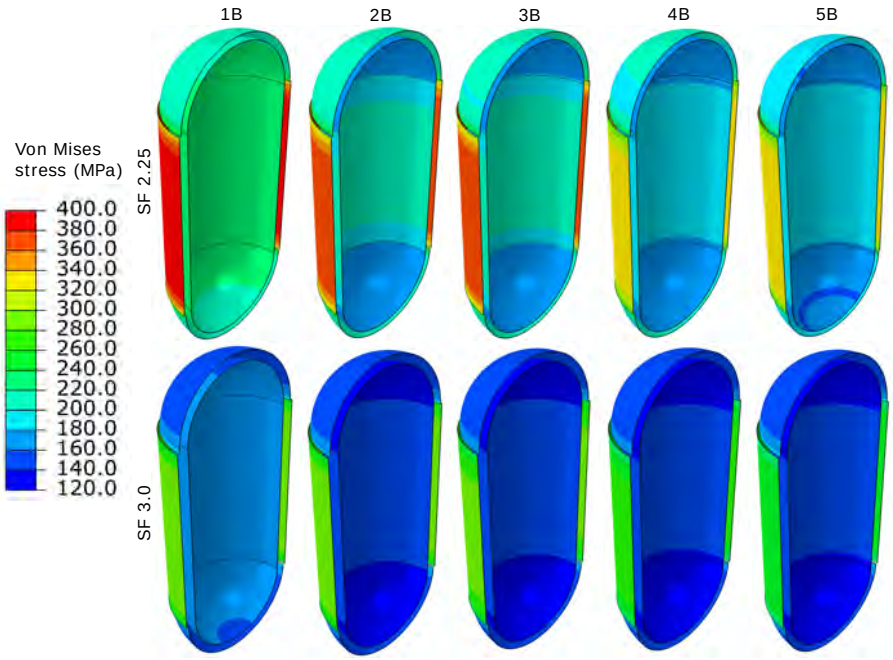

Figure 8: Von Mises stress contour plots for the first and last material layers for designs with hoop reinforcements for both safety factors subjected to 300 bar internal pressure.

3.2. Buckling analysis

As the AUV is designed to be submerged to depths up to 6000 m (600 bar external pressure), we need to understand the buckling behaviour and maximum pressure the pressure vessel can be subjected to. We have tested the most severe case, which is submerging an empty cylinder, i.e. no internal pressure. First, an eigenvalue buckling analysis was conducted for all optimised designs. The eigenvalue analysis only takes into account the linear behaviour of the material, disregarding any material or geometric nonlinearities. Hence, it produces an inaccurate result. However, running this method is an important part of the analysis as the resultant deformation can be used to "seed" material imperfections in the nonlinear buckling analysis.

The nonlinear analysis employs the modified Riks method [29], which solves simultaneously for loads and displacements. In this analysis, plasticity is taken into account and geometric imperfections were added from the previous eigen-

value analysis. Table 7 shows a comparison between the eigenvalue and nonlinear analyses, with the relative error being as high as 75%. This is in line with what is reported in the literature [30, 31, 32, 33].

Table 7: Eigenvalue and nonlinear buckling pressures for different designs and safety factors.

Safety factor 2.25				Safety factor 3.0			
Design	**Eigenvalue buckling pressure (bar)**	**Nonlinear buckling pressure (bar)**	**Relative error**	**Design**	**Eigenvalue buckling pressure (bar)**	**Nonlinear buckling pressure (bar)**	**Relative error**
1A	853	758	-13%	1A	1682	1531	-10%
2A	731	522	-40%	2A	1332	974	-37%
3A	764	496	-54%	3A	1371	886	-55%
4A	756	494	-53%	4A	1393	829	-68%
5A	770	491	-57%	5A	1389	824	-69%
1B	544	483	-13%	1B	1053	913	-15%
2B	675	464	-45%	2B	1210	834	-45%
3B	723	465	-56%	3B	1326	819	-62%
4B	771	499	-55%	4B	1378	809	-70%
5B	755	488	-55%	5B	1363	782	-74%

The radial displacement as a function of the external pressure for all optimised designs is shown in Figure 9. The buckling pressure for the higher safety factor version can be up to double the lower safety factor version, while the weight increase is only as high as 35%. Figure 10 shows a comparison between the buckling pressure for different designs. The designs without hoop reinforcement have a higher buckling resistance than their reinforced counterparts. However, this difference decreases as the thickness of the liner material increases. The main reason behind this behaviour is the nature of the buckling pressure, which is hydrostatic and hence equal in all directions. The hoop layers are placed only in one direction, and thus are greatly anisotropic. The helical layers, on the other hand, were placed at an angle with an antisymmetric stacking sequence and were optimised to distribute the stress around the pressure vessel evenly. The aluminium liner is an isotropic material, and hence the thicker it is, the more evenly the stresses are distributed around the pressure vessel. In addition, it is observed that the linerless designs without hoop reinforcement have a much greater resistance to buckling than the designs where the aluminium liner is present. This can be explained by Figure 6, which shows that due to the lack of liner, the designs without hoop reinforcement need more helical layers, leading to a much thicker and heavier layup. This leads to a bulkier pressure vessel, which is more resistant to buckling.

In order to safely fulfil the task of submerging to 6000 m, a design without

hoop reinforcement and safety factor of 3.0 is recommended. An intermediary configuration between designs 1A and 2A would be ideal, as the use of a linerless design is challenging due to high hydrogen permeation. A compromise between these designs would thus be ideal.

The buckling modes for designs without and with hoop reinforcements are shown in Figures 11 and 12 respectively. These deformation contours are the result from the simulations shown in Figure 9. All pressure vessels buckle in a similar way, with the buckling being concentrated in the cylinder area of the pressure vessel.

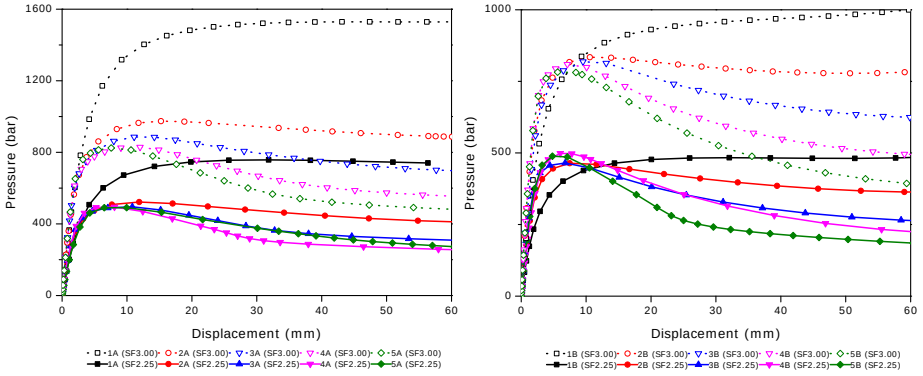

(a) (b)

Figure 9: Radial displacement as a function of external pressure for designs without hoop reinforcement (a), and with hoop reinforcement (b).

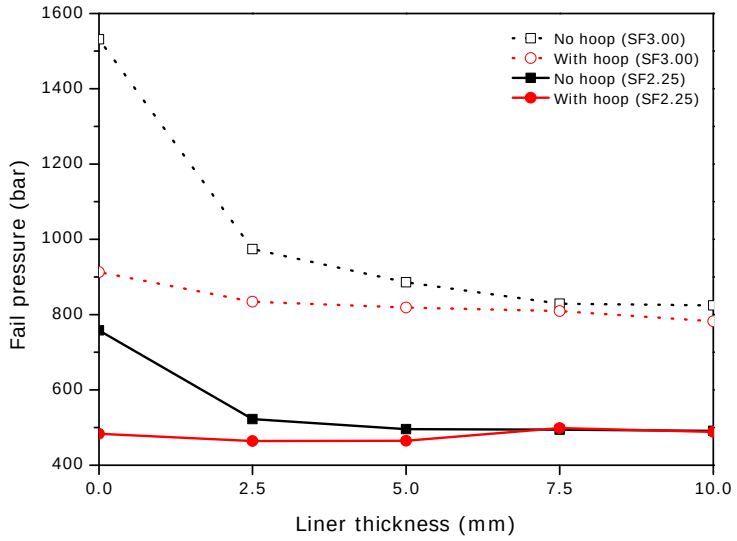

Figure 10: Fail pressure for different optimised designs (see Tables 5 and 6 for details).

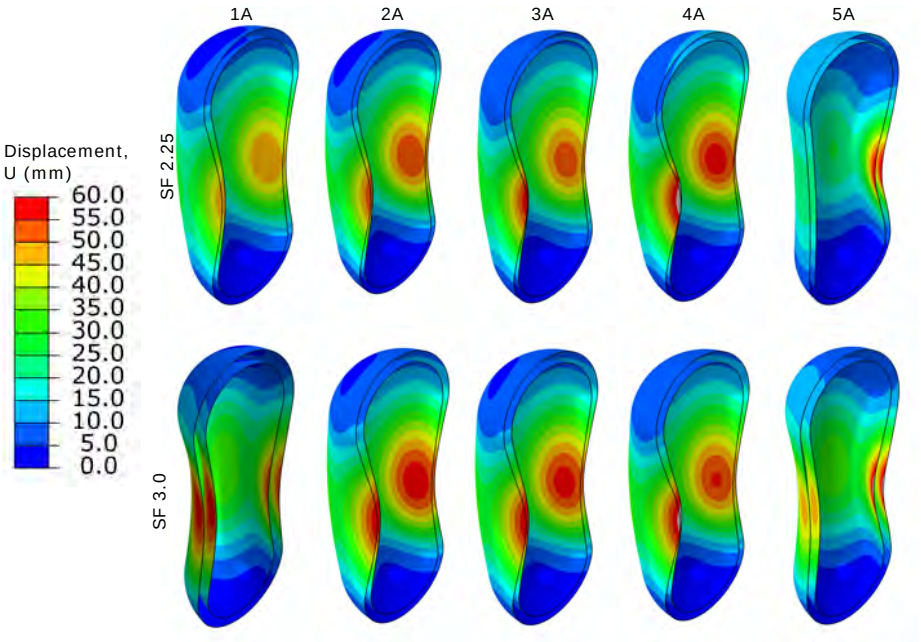

Figure 11: Buckling modes showing first and last material layers for designs without hoop reinforcements for both safety factors.

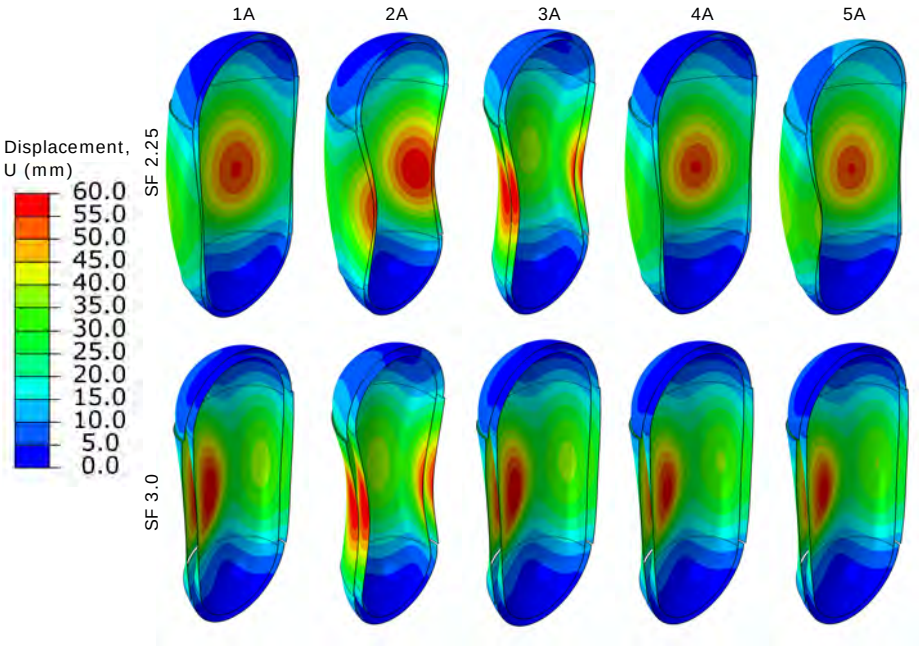

Figure 12: Buckling modes showing first and last material layers for designs with hoop reinforcements for both safety factors.

4. Conclusions

In this research paper we present a thorough finite element analysis of externally loaded type III hydrogen pressure vessels intended for underwater applications with operating working pressure conditions of 300 bar internal and up to 600 bar external pressure. A parametric analysis of several design parameters, including liner, helical, and hoop layer thickness, as well as wrapping helical angle was carried out for the working pressure condition. Several designs with different liner thicknesses were optimised so that the composite layer would be as thin as possible. For hoopless designs, the optimum helical angle of 50° was ideal for liners up to 5 mm thick, whereas from 5 to 10 mm thick liner an angle of 55° was found to be ideal. When hoop layers were present, a helical angle of 45° always provided the best thickness to safety factor ratio.

These optimised designs were then subjected to a buckling analysis, which

showed that the designs with a safety factor of 3.0 would be able to withstand the intended work depth of 6000 m without problems in the most severe loading condition (i.e. empty cylinder). We have found that designs without hoop reinforcements perform better under buckling, especially for liner thicknesses of 5 mm and lower. The analysis also shows that for the chosen designs, an increase in the liner thickness (of the pre-optimised designs) reduces the maximum external pressure that the pressure vessel can bear. Therefore, in order to maximise the external pressure bearable by the pressure vessel, an intermediary configuration between designs 1A and 2A is recommended.

Acknowledgements

The authors wish to express their gratitude to the European Commission for the financial support received through the European Union's Horizon 2020 research and innovation programme under grant agreement No 824348.

References

[1] V. L. Jantara Junior, Finite element analysis of deep-sea type III pressure vessels: raw and processed data, Mendeley Data, V1 (2020). doi:10.17632/hdxnbtkwb6.1.

[2] H. Barthelemy, M. Weber, F. Barbier, Hydrogen storage: recent improvements and industrial perspectives, International Journal of Hydrogen Energy 42 (11) (2017) 7254–7262. doi:10.1016/j.ijhydene.2016.03.178.

[3] R. Krishna, E. Titus, M. Salimian, O. Okhay, S. Rajendran, A. Rajkumar, J. Sousa, A. Ferreira, J. C. Gil, J. Gracio, Hydrogen storage for energy application, in: Hydrogen storage, IntechOpen, 2012, pp. 243–266.

[4] C. P. Fowler, A. C. Orifici, C. H. Wang, A review of toroidal composite pressure vessel optimisation and damage tolerant design for high pressure gaseous fuel storage, International Journal of Hydrogen Energy 41 (47) (2016) 22067–22089. doi:10.1016/j.ijhydene.2016.10.039.

[5] M. LeGault, The first commercial Type V composite pressure vessel, https://www.compositesworld.com/articles/next-generation-pressure-vessels, [Online; accessed 10-December-2020] (2020).

[6] J. Zheng, X. Liu, P. Xu, P. Liu, Y. Zhao, J. Yang, Development of high pressure gaseous hydrogen storage technologies, International Journal of Hydrogen Energy 37 (1) (2012) 1048–1057. doi:10.1016/j.ijhydene.2011.02.125.

[7] O. Comond, D. Perreux, F. Thiebaud, M. Weber, Methodology to improve the lifetime of type III HP tank with a steel liner, International Journal of Hydrogen Energy 34 (7) (2009) 3077–3090. doi:10.1016/j.ijhydene.2009.01.080.

[8] P. Xu, J. Zheng, H. Chen, P. Liu, Optimal design of high pressure hydrogen storage vessel using an adaptive genetic algorithm, International Journal of Hydrogen Energy 35 (7) (2010) 2840–2846. doi:10.1016/j.ijhydene.2009.05.008.

[9] P. Liu, J. Chu, S. Hou, J. Zheng, Micromechanical damage modeling and multiscale progressive failure analysis of composite pressure vessel, Computational Materials Science 60 (2012) 137–148. doi:10.1016/j.commatsci.2012.03.015.

[10] D.-S. Son, S.-H. Chang, Evaluation of modeling techniques for a type III hydrogen pressure vessel (70 MPa) made of an aluminum liner and a thick carbon/epoxy composite for fuel cell vehicles, International journal of hydrogen energy 37 (3) (2012) 2353–2369. doi:10.1016/j.ijhydene.2011.11.001.

[11] P. Liu, L. Xing, J. Zheng, Failure analysis of carbon fiber/epoxy composite cylindrical laminates using explicit finite element method, Composites Part B: Engineering 56 (2014) 54–61. doi:10.1016/j.compositesb.2013.08.017.

[12] L. Wang, C. Zheng, H. Luo, S. Wei, Z. Wei, Continuum damage modeling and progressive failure analysis of carbon fiber/epoxy composite pressure vessel, Composite Structures 134 (2015) 475–482. doi:10.1016/j.compstruct.2015.08.107.

[13] V. Alcantar, S. Ledesma, S. Aceves, E. Ledesma, A. Saldana, Optimization of type III pressure vessels using genetic algorithm and simulated annealing, International Journal of Hydrogen Energy 42 (31) (2017) 20125–20132. doi:10.1016/j.ijhydene.2017.06.146.

[14] B.-b. Liao, D.-l. Wang, L.-y. Jia, J.-y. Zheng, C.-h. Gu, Continuum damage modeling and progressive failure analysis of a Type III composite vessel by considering the effect of autofrettage, Journal of Zhejiang University-SCIENCE A 20 (1) (2019) 36–49. doi:10.1631/jzus.A1800152.

[15] M. Zhang, H. Lv, H. Kang, W. Zhou, C. Zhang, A literature review of failure prediction and analysis methods for composite high-pressure hydrogen storage tanks, International Journal of Hydrogen Energy 44 (47) (2019) 25777–25799. doi:10.1016/j.ijhydene.2019.08.001.

[16] S.-H. Hur, H.-J. Son, J.-H. Kweon, J.-H. Choi, Postbuckling of composite cylinders under external hydrostatic pressure, Composite Structures 86 (1-3) (2008) 114–124. doi:10.1016/j.compstruct.2008.03.028.

[17] C.-J. Moon, I.-H. Kim, B.-H. Choi, J.-H. Kweon, J.-H. Choi, Buckling of filament-wound composite cylinders subjected to hydrostatic pressure for underwater vehicle applications, Composite structures 92 (9) (2010) 2241–2251. doi:10.1016/j.compstruct.2009.08.005.

[18] H. Hernandez-Moreno, B. Douchin, F. Collombet, D. Choqueuse, P. Davies, Influence of winding pattern on the mechanical behavior of filament wound composite cylinders under external pressure, Composites Science and Technology 68 (3-4) (2008) 1015–1024. doi:10.1016/j.compscitech.2007.07.020.

[19] A. Siqueira Nóbrega de Freitas, A. Alfonso Alvarez, R. Ramos Jr, E. A. de Barros, Buckling analysis of an auv pressure vessel with sliding stiffeners, Journal of Marine Science and Engineering 8 (7) (2020) 515. doi:10.3390/jmse8070515.

[20] B. Cai, Y. Liu, Z. Liu, X. Tian, R. Ji, H. Li, Reliability-based load and resistance factor design of composite pressure vessel under external hydrostatic pressure, Composite Structures 93 (11) (2011) 2844–2852. doi:10.1016/j.compstruct.2011.05.020.

[21] A. Molavizadeh, A. Rezaei, Progressive damage analysis and optimization of winding angle and geometry for a composite pressure hull wound using geodesic and planar patterns, Applied Composite Materials 26 (3) (2019) 1021–1040. doi:10.1007/s10443-019-09764-8.

[22] ISO 19881:2018, Gaseous hydrogen - land vehicle fuel containers, BSI Standards Publication (2018).

[23] SIMULIA Abaqus 2017, Abaqus analysis user's guide (2017).

[24] D.-N. Zhang, Q.-Q. Shangguan, C.-J. Xie, F. Liu, A modified johnson–cook model of dynamic tensile behaviors for 7075-t6 aluminum alloy, Journal of Alloys and Compounds 619 (2015) 186–194. doi:10.1016/j.jallcom.2014.09.002.

[25] R. Rafiee, M. A. Torabi, Stochastic prediction of burst pressure in composite pressure vessels, Composite Structures 185 (2018) 573–583. doi:10.1016/j.compstruct.2017.11.068.

[26] T.-Y. Kam, Y. Liu, F. Lee, First-ply failure strength of laminated composite pressure vessels, Composite structures 38 (1-4) (1997) 65–70. doi:10.1016/S0263-8223(97)00042-1.

[27] O. Sayman, M. E. Deniz, T. Dogan, E. Yaylagan, Failure pressures of composite cylinders with a plastic liner, Journal of reinforced plastics and composites 30 (10) (2011) 882–888. doi:10.1177/0731684411412225.

[28] H. T. Hahn, S. W. Tsai, Introduction to composite materials, CRC Press, 1980.

[29] F. Abaqus, Abaqus inc, Providence, Rhode Island, United States (2017).

[30] G.-H. Koo, B. Yoo, J.-B. Kim, Buckling limit evaluation for reactor vessel of KALIMER liquid metal reactor under lateral seismic loads, International journal of pressure vessels and piping 78 (5) (2001) 321–330. doi:10.1016/S0308-0161(01)00049-7.

[31] R. Ng, A. Yousefpour, M. Uyema, M. G. Nejhad, Design, analysis, manufacture, and test of shallow water pressure vessels using e-glass/epoxy woven composite material for a semi-autonomous underwater vehicle, Journal of composite Materials 36 (21) (2002) 2443–2478. doi:10.1177/0021998302036021972.

[32] W. Xu, External pressure buckling analysis of large pressure vessels, in: Journal of Physics: Conference Series, Vol. 1303, IOP Publishing, 2019, p. 012019. doi:10.1088/1742-6596/1303/1/012019.

[33] T.-H. Joung, H.-J. Choi, S.-G. Lee, J.-M. Kim, J.-H. Lee, T.-C. Oh, A global buckling analysis of a pressure vessel associated with connections between main cylinder and flat plate ends, Ships and Offshore Structures 15 (4) (2020) 368–379. doi:10.1080/17445302.2019.1620974.